Slow dynamics, dynamic heterogeneities, and fragility of supercooled liquids confined in random media

doi: 10.1088/0953-8984/23/23/234123

Slow dynamics, dynamic heterogeneities, and fragility of supercooled liquids confined in random media

Kang Kim[1,2], **Kunimasa Miyazaki**[3], **and Shinji Saito**[1,2]

[1]Institute for Molecular Science, Okazaki 444-8585, Japan,
[2]The Graduate University for Advanced Studies, Okazaki 444-8585, Japan,
[3]Institute of Physics, University of Tsukuba, Tsukuba 305-8574, Japan

E-mail: kin@ims.ac.jp

Abstract. Using molecular dynamics simulations, we study the slow dynamics of supercooled liquids confined in a random matrix of immobile obstacles. We study the dynamical crossover from glass-like to Lorentz-gas-like behavior in terms of the density correlation function, the mean square displacement, the nonlinear dynamic susceptibility, the non-Gaussian parameter, and the fragility. Cooperative and spatially heterogeneous dynamics are suppressed as the obstacle density increases, which lead to the more Arrhenius-like behavior in the temperature dependence of the relaxation time. Our findings are qualitatively consistent with the results of recent experimental and numerical studies for various classes of spatially heterogeneous systems. We also investigate the dependence of the dynamics of mobile particles on the protocol to generate the random matrix. A reentrant transition from the arrested phase to the liquid phase as the mobile particle density *increases* is observed for a class of protocols. This reentrance is explained in terms of the distribution of the volume of the voids that are available to the mobile particles.

PACS numbers: 64.70.P-, 46.65.+g, 61.20.Lc

Submitted to: *J. Phys.: Condens. Matter*

1. Introduction

The transport properties of fluids in a heterogeneous environment are of great importance in physics, chemistry, and engineering [1, 2]. These systems include fluids confined in walls, standing thin-film liquids, and fluids adsorbed in random media. The effect of spatial confinement is especially important to the study of the glass transition of supercooled liquids. Recent experiments and computer simulations have revealed that the glass transition temperature, transport properties, and microscopic dynamics sensitively change in the presence of spatial confinement [3]. Moreover, it is expected that an understanding of these phenomena may lead to a deeper insight into the growing length scales of the cooperative motion of atoms, which escorts the drastic slowing down of dynamics near the glass transition point [4, 5]. A fluid in randomly distributed immobile obstacles is an ideal model to study the effects of the confinement on the glassy slow dynamics, in fact, a fluid in random media is interesting in its own right. This system is introduced as a model system of a crowded environment, and the transport phenomena contained within has attracted a great deal of attention in the biophysics community [6, 7, 8, 9]. This system can also be seen as a generalization of the Lorentz gas problem to the multi-particle case [10, 11, 12, 13]. Furthermore, this system can be regarded as a model of binary mixtures with a disparate size ratio [14, 15, 16, 17, 18, 19, 20, 21, 22, 23, 24]. The immobile obstacles in the random media are interpreted as large particles in the binary liquids because of the huge asymmetry in time scales between the small and large particle components.

In recent years, various molecular dynamics (MD) simulations have been performed to study the slow dynamics of the fluids in random media [25, 26, 27, 28, 29, 30, 31]. Theoretically, the slow dynamics of mobile hard spheres in the presence of the immobile hard spheres of the same size has been intensively investigated using the replica method combined with the mode-coupling theory (RMCT) [32, 33, 34, 35]. These studies have examined the dynamic phase transition from liquid to non-ergodic arrested states. Two notable results were predicted. The first is that the slow dynamics can be characterized by two types of dynamics: Type A and Type B dynamics [36]. When the mobile particle density, ρ_m, is large and the immobile particle density, ρ_i, is small, the system undergoes a conventional glass transition, in which the onset of slow dynamics is signaled by the *discontinuous* emergence of two-step relaxation in the density correlation function. This is referred to as Type B transition. As the immobile density ρ_i increases, the glass transition point of the mobile particles decreases drastically. At an even larger ρ_i, the dynamics qualitatively changes; one-step slow relaxation sets in at large wavelengths, in which the tail of the relaxation curve continuously grows and progressively propagates toward the smaller wavelengths as ρ_i increases, until the dynamics of the mobile particle freezes. This freezing is a localization transition due to blocking by the percolating network of the immobile particles. This is called Type A transition. The crossover from Type B to Type A transition is reminiscent of the behaviors observed in many heterogeneous systems such as the glass-to-gel crossover of attractive colloids [37, 38] and

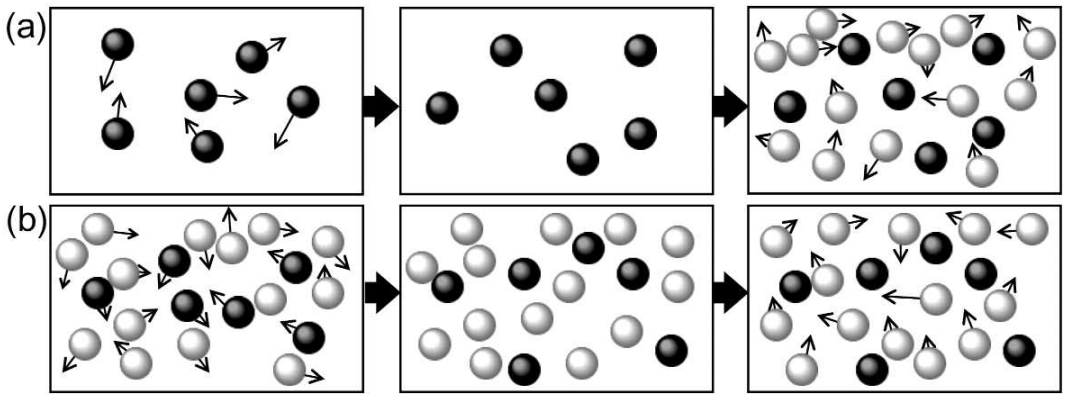

Figure 1. Schematic illustrations of two protocols to generate the random matrix: (a) Quenched-Annealed (QA) and (b) Equilibrated Mixture (EM) protocols.

the glassy slow dynamics of binary mixture systems with a disparate size ratio [16, 17]. The second prediction is the existence of a reentrant transition in the small ρ_m regime, in which the arrested mobile particles melt as the mobile particle density ρ_m *increases* at a fixed ρ_i.

To verify these theoretical predictions, we [39, 40] and Kurzidim *et al.* [41, 42] have independently and numerically investigated fluids in immobile obstacles. All of these studies have confirmed that there is a crossover from Type B to Type A transition as the immobile particle density increases. These studies also found no reentrant transition for the system that was studied by RMCT.

We have also found that the dynamic arrest line (or more precisely iso-relaxation-time line) sensitively depends on the protocol that is used to generate the configuration of the randomly distributed immobile particles [39, 40]. Two types of these protocols have been studied; the first is the Quenched-Annealed (QA) system, in which the immobile particles are initially equilibrated before their positions are quenched (see Fig. 1(a)). Mobile particles are then inserted into the system and their dynamics are monitored after equilibration. This QA protocol offers a natural choice to model the experimental setups of random media (such as porous materials) and has been adopted in the theoretical analysis of RMCT [32, 33, 34, 35] and in numerical studies by Kurzidim *et al.* [41, 42]. The second protocol studied is the Equilibrated Mixture (EM) protocol, in which all of the particles are run in the simulation box and, after their equilibration, the motions of a fraction of the particles are quenched (see Fig. 1(b)). The dynamics of the mobile component is monitored after waiting long enough for the mobile particles to equilibrate in the presence of the immobile particles. This protocol is appropriate as a model of the dynamics of the fast (small) particle component in binary mixtures with a disparate size ratio, in which the two time scales of each component are well separated. We found no reentrance for the system prepared with the QA protocol, but surprisingly, we did observe reentrance using the EM protocol [39, 40]. It should be noted that this reentrance is distinct from that predicted by RMCT. It was speculated that

this reentrance can be attributed solely to the configurations of the immobile particles prepared by the EM protocol; the configuration of immobile particles is automatically "optimized" to provide more pathways for the mobile particles than those prepared in the absence of mobile particles (using the QA protocol).

In the present paper, we investigate the dynamical properties of the fluids in random obstacles (which were also examined in our previous papers [39, 40]) in more detail, focusing on various quantities that characterize the slow dynamics near the glass and the localization transition. We evaluate the nonlinear dynamic susceptibility, the non-Gaussian parameter, and the fragility across the entire parameter space of (ρ_i, ρ_m). We also quantify how the dynamics of mobile particles sensitively depends on the protocol used to generate the random matrices.

This paper is organized as follows. In Sec. 2, we briefly review our model and simulation method. In Sec. 3, the numerical results are given; we first describe how the dynamics changes from Type B to Type A by calculating various dynamic quantities. In the latter subsection of Sec. 3, we discuss the sensitivity of the dynamics of mobile particles to a geometry of random configurations of the immobile particles by calculating the pore-size distribution. In Sec. 4, we summarize our results and provide our concluding remarks.

2. Model and methods

We perform MD simulations for two types of systems: a binary mixture interacting with the soft-core potential and a monodisperse hard sphere. The binary mixture is used to explore the entire parameter space of (ρ_i, ρ_m); bidispersity is required to avoid crystallization at the small obstacle density limit $\rho_i \to 0$. The monodisperse hard sphere is used to investigate the region at which the crossover from Type B to Type A transition takes place. This is also the region where the reentrant transition was predicted by RMCT. Monodispersity is of importance to explore the physical mechanism near the crossover without the risk of it being obscured by the softness of the potential or by the bidispersity of the system.

The binary soft-core mixture consists of an equal number of two types of particles with the total number $N = N_1 + N_2 = 500 + 500$. They interact via the soft-core potential

$$v_{\alpha\beta}(r) = \epsilon \left(\frac{\sigma_{\alpha\beta}}{r} \right)^{12}, \tag{1}$$

where $\sigma_{\alpha\beta} = (\sigma_\alpha + \sigma_\beta)/2$ and $\alpha, \beta \in \{1, 2\}$. The size and mass ratio were $\sigma_2/\sigma_1 = 1.2$ and $m_2/m_1 = 2$, respectively. The total number density was fixed at $\rho = (N_1+N_2)/L^3 = 0.8\sigma_1^{-3}$, in which the system length was $L = 10.77\sigma_1$ under periodic boundary conditions (PBC). The units of length, time, and temperature were considered to be σ_1, $\sqrt{m_1\sigma_1^2/\epsilon}$, and ϵ/k_B, respectively. For each simulation run, N_i particles were picked up from the N particles randomly and fixed their positions. $N_m = N - N_i$ particles were left mobile. In this model, we used the number densities defined by $\rho_i = N_i\rho_{\text{eff}}/N$ and

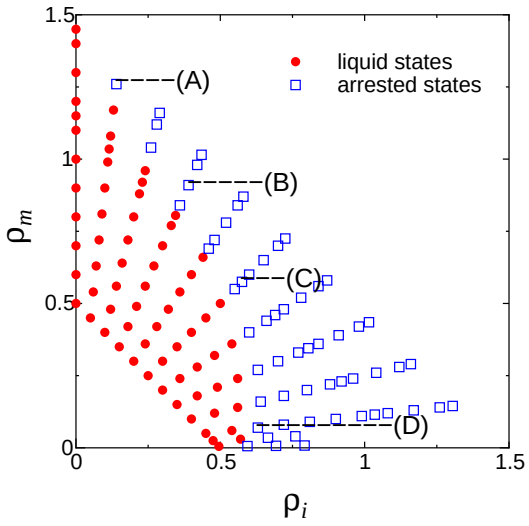

Figure 2. Dynamic phase diagram of the binary soft-core mixture generated by the EM protocol. ρ_i is the immobile (obstacle) particle density, and ρ_m is the mobile (fluid) particle density. The arrested states are defined as the points beyond which the α-relaxation time τ_α exceeds 10^3.

$\rho_m = N_m\rho_{\rm eff}/N$ as the system parameters, in which $\rho_{\rm eff} = N(\epsilon/k_BT)^{1/4}{\sigma_{\rm eff}}^3/V$ is the effective density of this model [43]. Here, $\sigma_{\rm eff}$ is the effective particle diameter defined by ${\sigma_{\rm eff}}^3 = \sum_{\alpha,\beta=1,2} x_\alpha x_\beta {\sigma_{\alpha\beta}}^3$, where $x_1 = N_1/N = 1/2$ and $x_2 = N_2/N = 1/2$ are the mixture compositions. The states that were investigated here were as follows: $\rho_{\rm eff} = 0.5$, 0.6, 0.7, 0.8, 0.9, 1.0, 1.1, 1.15, 1.2, 1.3, 1.4, and 1.45. The corresponding temperatures were as follows: $T = 21.61$, 10.42, 5.624, 3.297, 2.058, 1.350, 0.992, 0.772, 0.651, 0.473, 0.352, and 0.306, respectively. We controlled ρ_i and ρ_m by changing N_i (or N_m) and $\rho_{\rm eff}$ (or T). The number of mobile particles was chosen to be $N_m = 10 \sim 900$. The velocity Verlet algorithm was used to integrate Newton equations with time steps of $0.001 \sim 0.005$.

The monodisperse hard sphere system includes N identical hard spheres with mass m and diameter σ in a cubic box of volume V under PBC. σ and $\sqrt{m\sigma^2/k_BT}$ were used as the units of length and time, respectively. The temperature was fixed as $k_BT = 1$. The standard event-driven algorithm was used for particle collisions [44]. The number densities $\rho_i = N_i/V$ and $\rho_m = N_m/V$ were controlled by changing N_i, N_m, and V. For both systems, we carefully checked the system size dependence and the sample dependence of the observables throughout the study. Two types of protocols, the QA and EM protocols, were employed to generate the random matrices.

3. Numerical results

3.1. Dynamic phase diagram

We first determined the dynamic phase diagram for the whole (ρ_i, ρ_m)-space by performing MD simulations of the EM systems of the binary soft-core mixture. In

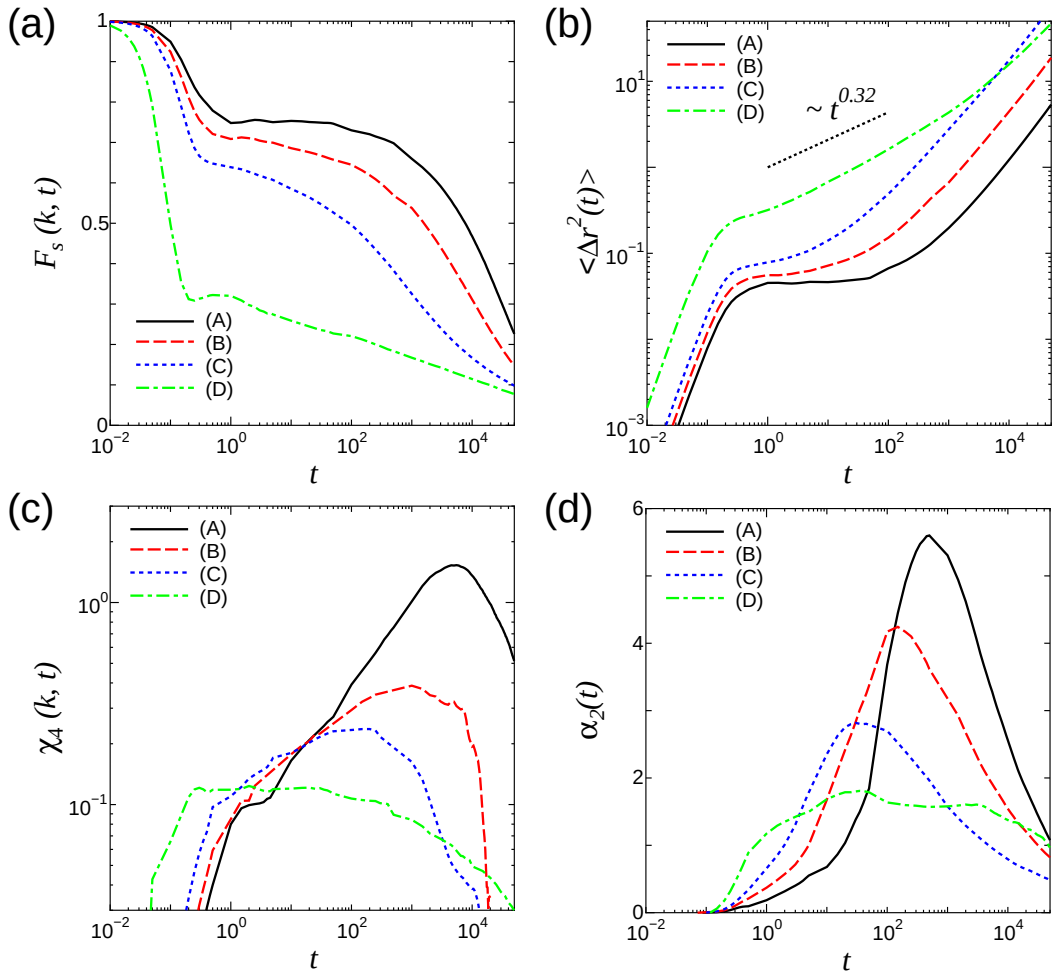

Figure 3. Various time-dependent quantities for the binary soft-core mixture generated by the EM protocol at the four state points (A) $(N_i, \rho_{\rm eff}) = (100, 1.45)$, (B) $(N_i, \rho_{\rm eff}) = (300, 1.3)$, (C) $(N_i, \rho_{\rm eff}) = (500, 1.15)$, and (D) $(N_i, \rho_{\rm eff}) = (900, 0.7)$, as denoted in Fig. 2. (a) the self-part of the intermediate scattering function $F_s(k,t)$ with $k = 2\pi$, (b) the mean square displacement $\langle \Delta r^2(t) \rangle$, (c) the nonlinear dynamic susceptibility $\chi_4(k,t)$ with $k = 2\pi$, and (d) the non-Gaussian parameter $\alpha_2(t)$.

Fig. 2, the dynamic phase diagram is plotted as a function of ρ_i and ρ_m. The dynamic arrest line is defined as the points at which the α-relaxation time τ_α reaches 10^3. We confirmed that varying the criteria for τ_α simply shifts the dynamic arrest line back and forth, but that its qualitative behavior remains intact. τ_α is determined by calculating the self-part of the intermediate scattering function for mobile particles,

$$F_s(k,t) = \frac{1}{N_m} \left\langle \sum_{j=1}^{N_m} \exp[i\vec{k} \cdot (\vec{r}_j(t) - \vec{r}_j(0))] \right\rangle, \tag{2}$$

where $\vec{k}$ is the wave vector, $k = |\vec{k}|$, and $\vec{r}_j(t)$ is the position of the j-th particle. We defined τ_α by $F_s(k = 2\pi, \tau_\alpha) = 0.1$.

As ρ_i increases, the dynamic arrest line (or the glass transition points) drastically decreases. These features were well documented in the previous simulations studies [28,

29, 30, 31] and in RMCT [32, 33, 34, 35]. This tendency is sustained up to the region, beyond which a small reentrant pocket is observed. This reentrance will be discussed in a later section.

3.2. Intermediate scattering function

The numerical results of conventional dynamical quantities displayed in Fig. 3 demonstrate how the immobile particle density ρ_i affects the relaxation processes of mobile particles. In Fig. 3(a), the time evolution of $F_s(k,t)$ with $k = 2\pi$ is plotted for the four state points (A)–(D) that are indicated in Fig. 2, at which the α-relaxation times are almost the same. The figure clearly indicates that there are two types of distinct dynamics depending on ρ_i.

In the small ρ_i (immobile particle density) regime $\rho_i \ll 0.5$, $F_s(k,t)$ exhibits two-step relaxation with a well-developed plateau, which is a hallmark of slow dynamics near the glass transition point. We found that the shoulder of the plateau discontinuously appears as one approaches from the fluid side to the arrested phase [39, 40]. This behavior is typical of slow dynamics near the glass transition point and is referred to as Type B transition in the MCT community. However, as the mobile particle density ρ_m decreases and ρ_i increases, the relaxation profile of $F_s(k,t)$ becomes quite different from that of Type B transition, *i.e.*, $F_s(k,t)$ shows a single step relaxation with a long tail (see $F_s(k,t)$ at the state (D)). It is also observed that the amplitude of the tail increases continuously as one crosses the arrested phase and that this increase incipiently starts from the lowest wavelength and propagates to the shorter scales as ρ_i increases [39, 40]. This behavior is known as the hallmark of Type A transition (or the localization transition) as predicted by RMCT [32, 33, 34, 35] and demonstrated by simulations for various spatially heterogeneous systems, such as binary mixtures of large and small particles [16, 17] and colloidal gels [37, 38].

3.3. Mean square displacement

The qualitative change from Type B to Type A dynamics is also observed in the mean square displacement (MSD) for mobile particles,

$$\langle \Delta r^2(t) \rangle = \frac{1}{N_m} \left\langle \sum_{j=1}^{N_m} |\vec{r}_j(t) - \vec{r}_j(0)|^2 \right\rangle . \tag{3}$$

The results are plotted in Fig. 3(b). It is known that in the Type B dynamics, the MSD exhibits a plateau at the β-relaxation time regime where the plateaus are observed for $F_s(k,t)$, in which the tagged particle is trapped by surrounding particles. However, at the small ρ_m limit (see (D) of Fig. 3(b)), anomalous subdiffusive behavior $\Delta r^2(t) \sim t^\alpha$ ($\alpha < 1$) is observed, in which the system is almost Lorentz-gas-like. On a short timeframe, the mobile particles at the state point (D) can explore longer distance than those at (A)–(C), because the mobile particle density is small. At a longer timeframe, however, the diffusion becomes very slow due to the developing network of immobile

particles that hinders the ability of the mobile particles to explore the long distance; this system can be explained in terms of the percolation theory [45]. The subdiffusion exponent $\alpha \approx 0.3$ is consistent with 0.32 predicted for the Lorentz gas [10, 11, 12, 13].

3.4. Nonlinear dynamic susceptibility

We next investigate the nonlinear dynamic susceptibility or four-point correlation function for mobile particles, $\chi_4(k,t)$, which is a measure that is used to quantify the extent of the dynamic heterogeneities [46, 47, 48]. $\chi_4(k,t)$ is defined as the variance of the fluctuations of the self part of the intermediate scattering function by

$$\chi_4(k,t) = N_m[\langle \hat{F}_s^2(k,t)\rangle - \langle \hat{F}_s(k,t)\rangle^2]. \tag{4}$$

Here $F_s(k,t) = \langle \hat{F}_s(k,t)\rangle$ and

$$\hat{F}_s(k,t) \equiv \frac{1}{N_m}\sum_{i=1}^{N_m} \frac{\sin(k|\Delta\vec{r}_i(t)|)}{k|\Delta\vec{r}_i(t)|}. \tag{5}$$

In the literatures [47], $N_m^{-1}\sum_{i=1}^{N_m}\cos(\vec{k}\cdot\Delta\vec{r}_i(t))$ is conventionally used as the definition of $\hat{F}_s(k,t)$. Under this definition, $\chi_4(k,t)$ decays to a constant 1/2 at $t\to\infty$. However, as we demonstrate here, the peak of $\chi_4(k,t)$ for the Type A regime grows more mildly than it does for the Type B regime. To demonstrate this suppression of the peak and thus the dynamic heterogeneities in the Type A regime without the results being obscured by a constant plateau at a large t, we have adopted an alternative definition of $\hat{F}_s(k,t)$ by taking the average over the angular components of the wave vector $\vec{k}$, which leads to eq.(5). Note that both definitions of $\hat{F}_s(k,t)$ lead to an identical averaged value $F_s(k,t) = \langle \hat{F}_s(k,t)\rangle$ due the isotropic nature of the system, but that the new definition removes the unwanted constant for $\chi_4(k,t)$ at $t\to\infty$. In Fig. 3(c), the time evolutions of $\chi_4(k,t)$ are plotted for the four state points (A)–(D). In the Type B regime, $\chi_4(k,t)$ exhibits behavior that is typical for bulk glass, *i.e.*, a pronounced peak at the α-relaxation time, whose height grows rapidly as the density increases and is preceded by algebraic growth in the β-relaxation regime. In the Type A regime at state (D), however, $\chi_4(k,t)$ neither grows nor shows a strong peak, even after a long period of time. This results implies that dynamic heterogeneities play a minor role in the slow dynamics of this regime. Similar behavior of $\chi_4(k,t)$ has been reported for colloidal gels whose slow dynamics are caused by geometrical constraints [49, 50].

3.5. Non-Gaussian parameter

The non-Gaussian parameter (NGP) is another typical quantity that is suitable to monitor the effect of the heterogeneities inherent in the system. We calculated the NGP $\alpha_2(t)$ defined by

$$\alpha_2(t) = \frac{3\langle \Delta r^4(t)\rangle}{5\langle \Delta r^2(t)\rangle^2} - 1, \tag{6}$$

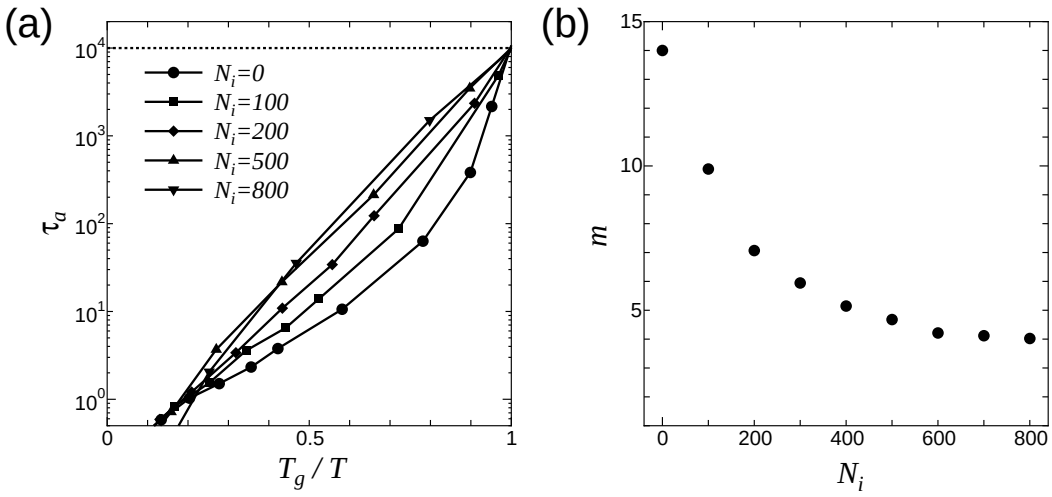

Figure 4. (a) The α-relaxation time, τ_α, as a function of the inverse temperature T_g/T, for several N_i's, $N_i = 0$, 100, 200, 500 and 800. T_g is defined as the temperature at which $\tau_\alpha = 10^4$. (b) N_i-dependence of the fragility index m.

where $\langle \Delta r^4(t) \rangle = (1/N_m) \langle \sum_{j=1}^{N_m} |\vec{r}_j(t) - \vec{r}_j(0)|^4 \rangle$. $\alpha_2(t)$ reveals how the distribution of the single-particle displacement, $|\Delta \vec{r}_j(t)|$, at time t deviates from the Gaussian distribution [51]. The profiles of $\alpha_2(t)$ are indicated in Fig. 3(d).

It is observed that $\alpha_2(t)$ develops and exhibits the pronounced peak before the α-relaxation time in the Type B regime. It is known that an increase in the maximum $\alpha_2(t)$ is synchronized with the growing *dynamic* heterogeneities near the glass transition point [52]. As the immobile density ρ_i increases, the height of the peak decreases. At the largest ρ_i, the point (D), it is hard to see the peak. This trend is qualitatively similar to that of the nonlinear dynamic susceptibility, $\chi_4(k,t)$. Recently, Flenner and Szamel have proposed a new non-Gaussian parameter (NNGP) [53]. They argued that the conventional NGP is more susceptible to particles moving faster than those moving more slowly, whereas NNGP is more susceptible to slowly moving particles. It would be beneficial to compute and compare the NGP, NNGP, and $\chi_4(k,t)$ in order to corroborate the role of the dynamic and static heterogeneities in the confined systems.

3.6. Fragility

The "fragility" is a concept to quantify the deviation of the temperature dependence of the viscosity, diffusion coefficient, and the relaxation time from the Arrhenius behavior [54]. The fragility index m is commonly used as a measure of the fragility and is defined by the steepness of the increase of τ_α upon decreasing the temperature;

$$m = \frac{\partial \log_{10} \tau_\alpha}{\partial (T_g/T)} \Big|_{T=T_g}, \tag{7}$$

where T_g is the glass transition point. m depends on the material of the glass formers. Generally, fragile liquids with large m's tend to exhibit more pronounced and more temperature-sensitive dynamic heterogeneities than do more Arrhenius-like fluids with

smaller m's (or stronger liquids). As was demonstrated in the previous sections, the dynamic heterogeneities are suppressed as the immobile particle density ρ_i increases. Therefore, it is natural to expect that the system concomitantly becomes stronger (more Arrhenius-like). We examined the temperature (or the effective density $\rho_{\rm eff}$) dependence of τ_α's for various N_i's (the number of the immobile particles) for a binary soft-core mixture. Note that we have used $\rho_{\rm eff}$ to control T. The change of $\rho_{\rm eff}$ changes ρ_i (and also ρ_m) slightly, and this shift may make it difficult to quantify the effects of the fixed number of obstacles on the fragility. We believe, however, that this effect is negligible for the range of the temperatures that we have explored.

The "Angell-plot", the $\log_{10}\tau_\alpha$-vs-$1/T$ plot, of our system is shown in Fig. 4(a), in which the temperature T is scaled by the "glass transition temperature" T_g. T_g has been defined by the point at which τ_α reaches 10^4 that is slightly longer than the criteria used to draw Fig. 2. The dependence of the fragility index m on the number of immobile particles N_i is plotted in Fig. 4(b). We observe that m is remarkably sensitive to the density of immobile particles. The fragility index is $m \approx 14$ for bulk glass but it decreases to $m \approx 4$ at the largest density of immobile particles. Our observation differs from the one reported for a binary mixture system with large size ratios (≤ 3) by Kurita *et al.* [24]. They indicated that the fragility changed non-monotonically, though mildly, by changing the size ratio of small and large particles and their densities. It would be interesting to study how this trend changes as the size ratio of the two components increases, resulting in the time scales for each component becoming decoupled.

We remark that the fragility, which behaves in a manner that is qualitatively similarly to ours, has been experimentally obtained in polymeric systems confined in porous media recently [55], in which the crossover from a non-Arrhenius to Arrhenius temperature-dependence of the relaxation time was observed as the pore size became smaller. It was speculated that the decrease of the fragility as the effect of the confinement is enhanced is universal and should be observed for other types of confined systems such as those with the solid-liquid or air-liquid interfaces [56].

Finally, it should be noted that even the largest values of m reported here are still very small compared with conventional molecular systems [57]. This discrepancy occurs because the glass transition temperature T_g defined above is far higher than those observed for real glasses, which is due to the limited time windows that the simulations can access. It is noteworthy that our simulation results still exhibited qualitatively similar behavior for m as the experimental results, despite the large time-scale differences between them.

3.7. Reentrant transition

In this subsection, we examine the effect of the configurations of immobile particles on dynamics of the mobile particles by comparing results obtained with the EM protocol to those obtained with the QA protocol in the monodisperse hard sphere system. We used the one-component hard spheres to study the mechanism behind the configuration-

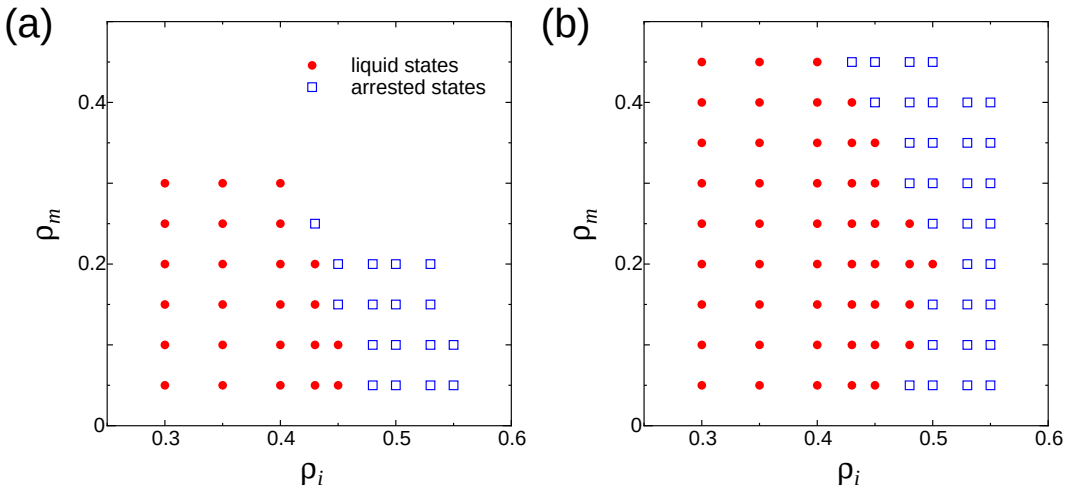

Figure 5. Dynamic phase diagram of the monodisperse hard sphere system with a random matrix generated by the two different protocols: (a) QA and (b) EM.

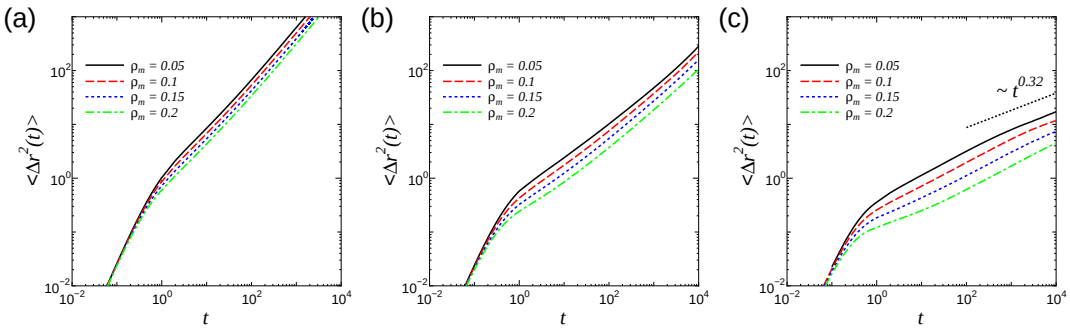

Figure 6. The ρ_m dependence of the mean square displacement, $\langle \Delta r^2(t) \rangle$, at the immobile particle density (a) $\rho_i = 0.3$, (b) 0.43, and (c) 0.5 of the QA systems

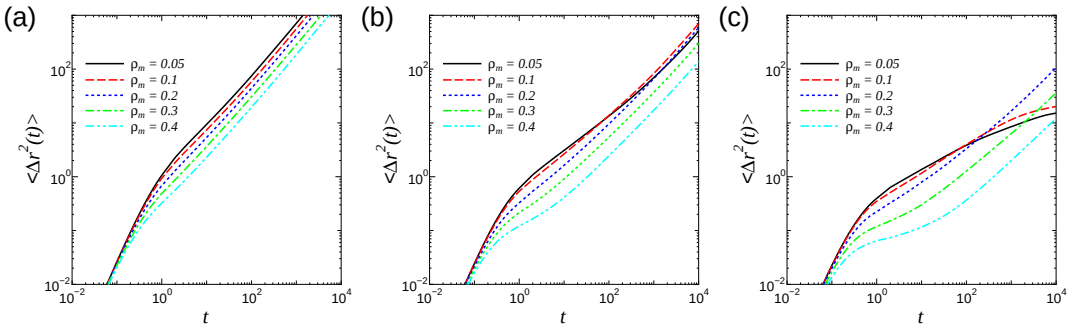

Figure 7. The ρ_m dependence of the mean square displacement, $\langle \Delta r^2(t) \rangle$, at the immobile particle density (a) $\rho_i = 0.3$,(b) 0.43, and (c) 0.5 of the EM systems.

dependence of dynamics near the Type B-Type A crossover without the results being obscured by the softness of the potential or by the bidispersity of the system. We calculated the MSD of the mobile particles and determined the dynamic phase diagrams for both the QA and EM systems. The results are plotted in Fig. 5. Here, the dynamic

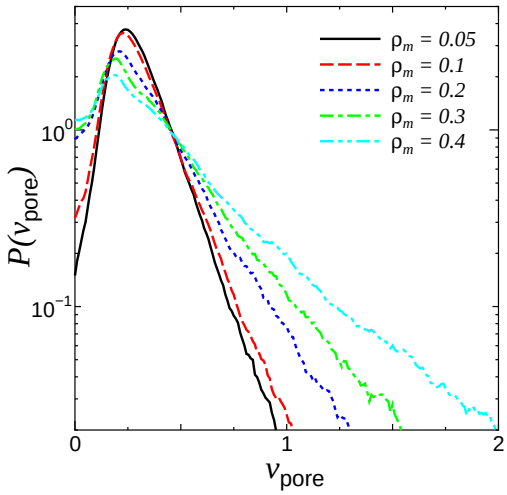

Figure 8. The pore-size distribution $P(v_{\rm pore})$ for various mobile particle densities ρ_m at the fixed immobile particle density $\rho_i = 0.5$ of the EM systems.

arrest line is determined as the points at which the MSD reaches 10^2 in the simulation time $t = 10^4$. Figs. 6 and 7 show the dependence of the MSD on ρ_m at several ρ_i's for both the QA and EM systems.

As indicated by Fig. 5(a), *no* reentrant transition is observed for the QA system. The dynamic arrest line monotonically decreases as ρ_i increases, which is compatible with the recent numerical simulations for the related QA systems [41, 42]. Indeed, Fig. 6 indicates that the slope of the MSD monotonically decreases as ρ_m increases at a fixed ρ_i. On the one hand, this result is hardly surprising because the slowing down of the mobile particle dynamics is mainly due to the geometrical confinement by the immobile particles. On the other hand, the EM system shows the reentrant pocket at a finite ρ_m, which is clearly seen in Fig 5(b). The similar reentrance pocket has been observed in the binary soft-core mixture (see Fig. 2). The dynamics of the mobile particles are *accelerated* in spite of the increase in ρ_m. This reentrance can be clearly seen in Fig. 7(b) and (c); by increasing ρ_m at the fixed large ρ_i, the slope of the MSD at long times first *increases* and then gradually decreases.

In our previous study [39, 40], we have speculated that the origin of this reentrance is due to the change of the equilibrium structure of the immobile particles in the presence of the mobile particles, which are equilibrated together when the random matrix is generated. To verify this speculation, we investigated the distribution of the pore size (or the free volume available for the mobile particles) generated by the immobile particles. The pore-size distribution is determined as follows. Using a three dimensional Delaunay triangulation algorithm, the total space of the system is divided into non-overlapping tetrahedrons. The vertices consist of the positions of the immobile particles. The volume distribution of the tetrahedrons, $P(v_{\rm pore})$, for EM systems is computed. If the volume of the tetrahedron is much larger than that of the particle, $v_{\rm pore} > \pi\sigma^3/6 \simeq 0.52\sigma^3$, the mobile particle can access the pore. The available pore-sizes for the mobile particles are

not identical to the available pathways that are available to them, but their distribution function still provides reliable information on the dynamics of the mobile particles in geometrical confinement. As observed in Fig. 8, the height of the tail of $P(v_{\rm pore})$ at $v_{\rm pore} \geq 0.52\sigma^3$ *increases* as ρ_m *increases* at a fixed value of $\rho_i = 0.5$ monotonically. This result indicates that the free volumes available for the mobile particles increases, which leads to the reentrant behavior of the MSD that is observed in Fig. 7(c). Note that the tails monotonically increase (at least up to $\rho_m = 0.4$), but the dynamics slow down again around $\rho_m \approx 0.2$, as indicated by Fig. 5(b). This result occurs because the glassy dynamics of the mobile particles sets in while the localization effect (due to the geometrical confinements) becomes smaller.

These results quantify our speculation that the immobile particles adjust themselves during an equilibration run to prepare for the presence of the mobile particles so that the free volumes for both components are entropically maximized and leave more available geometrical spaces (and pathways) for the mobile particles, delaying the percolation transition to larger values and thus leading to faster dynamics of the mobile particles. The sensitivity of the percolation point to the protocols used to generate the matrix configuration has been previously studied in several contexts and our results are consistent with these results [29, 30, 31].

We also speculate that counterintuitive effects similar to the reentrance discussed above are prevalent in systems in which the disparate time scales are entangled. A binary mixture consisting of large and small particles studied by MD simulations may be a good example. Voigtmann *et al.* have numerically studied the dynamics of such a binary mixture and have shown that the diffusion of small particles becomes slower when the interactions between small particles are turned off [22, 23]. One may speculate that this observation is relevant to our finding of the reentrant pocket for the EM system. The turn-off of the interactions makes small particles "invisible" to each other and makes the large particles behave as if there are fewer small particles around them, which makes the configuration of the large particles become more QA-like than those with full interactions. This effect might be difficult to observe via standard static quantities (such as the static structure factors) but may be detected easily via the pore-size distribution function. An accurate theoretical method to evaluate the subtle differences in the static structure factors would be desirable to investigate how the protocol dependence changes the dynamic phase diagram using RMCT [58].

4. Conclusions

In this paper, MD simulations have been performed to examine the dynamical properties near the arrest points of simple fluids confined in random media. We calculated various quantities for the whole range of the mobile and immobile densities, including the intermediate scattering function, the mean square displacement, the nonlinear dynamic susceptibility, the non-Gaussian parameter, and the fragility. We found that all of these quantities exhibited qualitative changes as the density of the mobile/immobile particles

was varied. At the limit of small immobile particle density, all of the observed quantities indicated the strong signs of dynamic heterogeneities near the glass transition point, such as the enhanced nonlinear dynamic susceptibility, the increased peak heights of the non-Gaussian parameter, and the fragile behavior of the relaxation time in its temperature dependence. At the opposite limit, in which a small number of mobile particles diffuse amid abundant obstacle particles, the signs of the dynamic heterogeneities were all suppressed. The nonlinear dynamic susceptibility and the non-Gaussian parameter exhibited no peak, and the temperature dependence of the relaxation time was almost Arrhenius. To understand the underling physics behind the reentrant transition near the Type B to Type A crossover, we have carefully quantified how the statistical properties of configuration of the random matrix can be altered by the different protocols used to generate them by calculating the pore-size distribution generated by the immobile particles. Throughout this paper, we refer the change from Type B to Type A dynamics as the crossover. According to RMCT [32, 33, 34, 35], this change should be associated with a higher order MCT transition. However, this transition is too subtle to be clearly observed at the resolution of the current simulations.

Acknowledgments

This work was partially supported by Grants-in-Aid for Scientific Research: Young Scientists (B) (Grant No. 21740317), Scientific Research (B) (Grand No. 22350013), Scientific Research (C) (Grand No. 21540416) and Priority Area "Soft Matter Physics." This work was also supported by the Center for the Promotion of Integrated Sciences (CPIS) of Sokendai and the Next Generation Super Computing Project, Nanoscience Program, MEXT, Japan. The numerical calculations were performed at Research Center for Computational Science, Okazaki Research Facilities, National Institutes of Natural Sciences, Japan.

References

[1] Havlin S and Ben-Avraham D 2002 *Adv. Phys.* **51** 187
[2] Alba-Simionesco C, Coasne B, Dosseh G, Dudziak G, Gubbins K E, Radhakrishnan R and Sliwinska-Bartkowiak M 2006 *J. Phys.: Condens. Matter* **18** R15
[3] Alcoutlabi M and Mckenna G B 2005 *J. Phys.: Condens. Matter* **17** R461
[4] Scheidler P, Kob W and Binder K 2002 *Europhys. Lett.* **59** 701
[5] Biroli G, Bouchaud J P, Cavagna A, Grigera T S and Verrocchio P 2008 *Nat. Phys.* **4** 771
[6] Saxton M 1994 *Biophys. J.* **66** 394
[7] Saxton M J and Jacobson K 1997 *Annu. Rev. Biophys. Biomol. Struct.* **26** 373
[8] Ellis R J and Minton A P 2003 *Nature* **425** 27
[9] Sung B J and Yethiraj A 2008 *J. Phys. Chem. B* **112** 143
[10] Höfling F, Franosch T and Frey E 2006 *Phys. Rev. Lett.* **96** 165901
[11] Höfling F and Franosch T 2007 *Phys. Rev. Lett.* **98** 140601
[12] Höfling F, Munk T, Frey E and Franosch T 2008 *J. Chem. Phys.* **128** 164517
[13] Bauer T, Höfling F, Munk T, Frey E and Franosch T 2010 *Euro. Phys. J. Special Topics* **189** 103
[14] Imhof A and Dhont J K G 1995 *Phys. Rev. Lett.* **75** 1662

[15] Dinsmore A D, Yodh A G and Pine D J 1995 *Phys. Rev. E* **52** 4045
[16] Moreno A J and Colmenero J 2006 *Phys. Rev. E* **74** 021409
[17] Moreno A J and Colmenero J 2006 *J. Chem. Phys.* **125** 164507
[18] Kikuchi N and Horbach J 2007 *Europhys. Lett.* **77** 26001
[19] Horbach J, Kob W and Binder K 2002 *Phys. Rev. Lett.* **88** 125502
[20] Voigtmann T and Horbach J 2006 *Europhys. Lett.* **74** 459
[21] Mayer C, Sciortino F, Likos C N, Tartaglia P, Löwen H and Zaccarelli E 2009 *Macromolecules* **42** 423
[22] Voigtmann T and Horbach J 2009 *Phys. Rev. Lett.* **103** 205901
[23] Horbach J, Voigtmann T, Höfling F and Franosch T 2010 *Euro. Phys. J. Special Topics* **189** 141
[24] Kurita R and Weeks E R 2010 *Phys. Rev. E* **82** 041402
[25] Gallo P, Pellarin R and Rovere M 2002 *Europhys. Lett.* **57** 212
[26] Gallo P, Pellarin R and Rovere M 2003 *Phys. Rev. E* **67** 041202
[27] Gallo P, Pellarin R and Rovere M 2003 *Phys. Rev. E* **68** 061209
[28] Kim K 2003 *Europhys. Lett.* **61** 790
[29] Chang R, Jagannathan K and Yethiraj A 2004 *Phys. Rev. E* **69** 051101
[30] Mittal J, Errington J R and Truskett T M 2006 *Phys. Rev. E* **74** 040102(R)
[31] Sung B J and Yethiraj A 2008 *J. Chem. Phys.* **128** 054702
[32] Krakoviack V 2005 *Phys. Rev. Lett.* **94** 065703
[33] Krakoviack V 2005 *J. Phys.: Condens. Matter* **17** S3565
[34] Krakoviack V 2007 *Phys. Rev. E* **75** 031503
[35] Krakoviack V 2009 *Phys. Rev. E* **79** 061501
[36] Götze W 1991 Aspects of structural glass transitions *Liquids, Freezing and the Glass Transition* ed Hansen J P, Levesque D and Zinn-Justin J (North-Holland, Amsterdam) pp 287–503
[37] Zaccarelli E, Voivod S I, Buldyrev S V, Moreno A J, Tartaglia P and Sciortino F 2006 *J. Chem. Phys.* **124** 124908
[38] Zaccarelli E 2007 *J. Phys.: Condens. Matter* **19** 323101
[39] Kim K, Miyazaki K and Saito S 2009 *EPL* **88** 36002
[40] Kim K, Miyazaki K and Saito S 2010 *Euro. Phys. J. Special Topics* **189** 135
[41] Kurzidim J, Coslovich D and Kahl G 2009 *Phys. Rev. Lett.* **103** 138303
[42] Kurzidim J, Coslovich D and Kahl G 2010 *Phys. Rev. E* **82** 041505
[43] Yamamoto R and Onuki A 1998 *Phys. Rev. E* **58** 3515
[44] Allen M P and Tildesley D J 1989 *Computer Simulation of Liquids* (Oxford University Press, USA)
[45] Stauffer D and Aharony A 1994 *Introduction to Percolation Theory* (CRC Press)
[46] Glotzer S C, Novikov V N and Schroder T B 2000 *J. Chem. Phys.* **112** 509
[47] Toninelli C, Wyart M, Berthier L, Biroli G and Bouchaud J P 2005 *Phys. Rev. E* **71** 041505
[48] Biroli G, Bouchaud J P, Miyazaki K and Reichman D R 2006 *Phys. Rev. Lett.* **97** 195701
[49] Abete T, de Candia A, Del Gado E, Fierro A and Coniglio A 2007 *Phys. Rev. Lett.* **98** 088301
[50] Fierro A, Del Gado E, de Candia A and Coniglio A 2008 *J. Stat. Mech.* L04002
[51] Hansen J P and Mcdonald I R 2006 *Theory of Simple Liquids, Third Edition* (London: Academic Press)
[52] Kob W, Donati C, Plimpton S J, Poole P H and Glotzer S C 1997 *Phys. Rev. Lett.* **79** 2827
[53] Flenner E and Szamel G 2005 *Phys. Rev. E* **72** 011205
[54] Angell C A 1991 *J. Non-Crys. Solids* **131-133** 13
[55] Schönhals A, Goering H, Schick C, Frick B, Mayorova M and Zorn R 2007 *Euro. Phys. J. Special Topics* **141** 255
[56] Inoue R, Kanaya T, Nishida K, Tsukushi I, Telling M T F, Gabrys B J, Tyagi M, Soles C and Wu 2009 *Phys. Rev. E* **80** 031802
[57] Böhmer R, Ngai K L, Angell C A and Plazek D J 1993 *J. Chem. Phys.* **99** 4201
[58] Krakoviack V 2010 *Phys. Rev. E* **82** 061501